Real-time soil compaction monitoring through pad strain measurements: modeling to inform strain gage placement

Shawn C. Kimmel, Colorado School of Mines
Michael A. Mooney, Colorado School of Mines

ABSTRACT

Soil compaction monitoring is critical to earthwork projects, including roadways, earth dams, and levees. Current methods require a halt of production, and provide at best sparse coverage. A system is proposed for static pad foot soil compaction to provide real-time feedback at higher spatial resolutions through machine integrated sensors. The system is composed of pad sensors that measure total normal force and contact stress distribution (CSD), laser sensors that measure soil deflection, and GPS to spatially reference measurements. By combining these measurements, soil stiffness and potentially modulus can be determined. This paper discusses the development of the force and CSD sensing pad. The concept is to instrument individual pads with strain gages to determine loading conditions. Modeling is used to inform strain gage positioning through pad strain behavior analysis of different simulated soil conditions. The finite element analysis (FEA) of a Caterpillar pad is discussed, including formulation and rationale for the various model parameters. In particular, the loading parameters are explained and include the range of force magnitudes experienced throughout compaction and the CSD elicited by various soils. The results of this analysis are presented, and show that pad strain is sensitive to both force magnitude and CSD. Specific strain trends are identified in the sidewall and bottom face of the pad which are particularly sensitive to the loading variables. Strain gage placements are proposed that capture the identified trends, thereby providing definitive information on total normal force and CSD.

Keywords: Intelligent Soil Compaction Monitoring Finite Element Modeling Strain Experimental Instrumentation

1 INTRODUCTION

Real-time soil compaction monitoring represents a significant leap forward in the quality assessment of earthen structures and foundations. Without this technology, compaction monitoring feedback takes the form of time consuming quality control/ quality assurance (QC/QA) spot tests that halt production and provide less than 0.1% coverage of the area[1]. For several soil compaction applications, real-time soil stiffness monitoring technologies already exist. This includes smooth drum vibratory compaction[1,2] and high energy impact compaction[3]. Caterpillar has developed a relative measure of soil compaction based on machine drive power that works for static rollers[4]. However, there is currently no real-time soil stiffness monitoring technology for static pad foot compaction.

Figure 1. Concept of real-time soil compaction monitoring for static pad foot rollers. Wireless instrumented pads provide soil stiffness measurements, which are spatially referenced by GPS and provided to the operator via an onboard computer and monitor.

This paper discusses the development of real-time soil stiffness monitoring for static pad foot rollers in the form of built-in pad sensors (pads are the protrusions on the drum surface of the compactor as shown in Figure 1). The concept of this measurement system is shown in Figure 1. Wireless sensors in the pads provide continuous measurements of total normal force, which are spatially referenced by GPS. Laser sensors measure soil deformation that can be combined with pad measurements to provide soil stiffness. An onboard computer processes this information and provides it to the machine operator, site management, and QC/QA personnel to provide decision making support and as-built documentation. One key to this technology is the development of a pad sensor that provides a measure of total normal force.

In order to measure soil compaction, the pad sensor must detect changes in the pad-soil interaction. As soil stiffens during the compaction process, the drum begins to "walk-out" of the soil as shown in Figure 2. Stiffer soil will result in less soil deformation and fewer pads supporting the weight of the drum. It follows that the loading on individual pads will change with compaction. The ideal pad sensor would be able to track this phenomenon, providing definitive information on compaction and applied force.

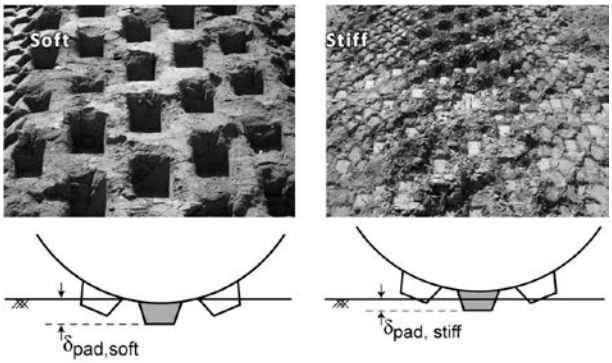

Figure 2. As soil is compacted, the drum "walks-out" of the soil producing shallower indentations. It is expected that the loading of each pad will change in conjunction with this phenomenon.

The research discussed herein pursues the use of strain gages as transducers for detecting this change in the loading of individual pads throughout compaction. This strain gage based method of instrumentation is similar to the use of strain gages as transducers in load cells. However, a key difference in load cells is the simplicity of their geometry, which allows for the extraction of force through simple analytical solutions. Conversely, the pad geometry and soil loading is too complex for a simple analytical solution. Instead, numerical modeling in the form of finite element (FE) analysis is employed to gain insight into pad strain behavior, and identify locations for strain gages that are sensitive to loading.

This paper introduces the FE model, presents FE analysis results, and discusses features of pad strain behavior observed during modeling. The FEA results are used to identify discrete locations of interest for placing strain gages.

2 MODELING OF A PAD COMPACTING SOIL

In order to investigate pad strain behavior spatially under various loading conditions, pads from multiple manufacturers were analyzed using numerical methods. This section discusses important modeling parameters, and how they were derived. Specifically, the most challenging aspect in this modeling application was determining how to apply loads to represent the range of conditions experienced in the field. This was accomplished with the help of field observation and theoretical and experimental knowledge of soil mechanics.

Pads from multiple manufacturers (Caterpillar, Bomag) were modeled in SolidWorks® 3D CAD software. FE analysis was performed with the SolidWorks® Simulation package. The pad model meshes are shown in Figure 3. The standard Solidworks® mesh was used, which employs tetrahedral elements. For the BOMAG pad, the mesh achieved 99.9% of elements with an aspect ratio less than 3 and a maximum of 4.6; for the Caterpillar pad, the mesh achieved 97.3% of elements with an aspect ratio less than 3, and a maximum of 8.5. For simplicity, a single pad design (of the Caterpillar pad) is presented in this paper. However, the various pad designs share common elements, such as a trapezoidal profile and hollow center, which allow the model parameters and findings to transport well between designs.

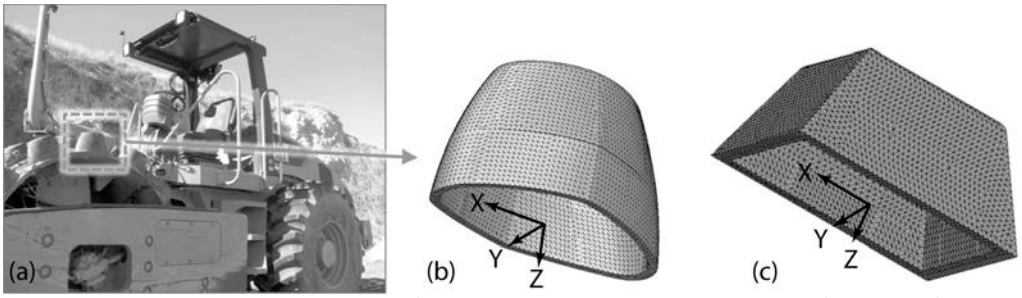

Figure 3. A soil compactor drum (a) possesses dozens of pads (protrusions welded to the drum surface). Pads from two manufacturers were modeled in SolidWorks®. This shows the meshes for (b) the Caterpillar pad model and (b) the BOMAG pad model.

For simplicity, the FE modeling simulated vertical loading of the pad into soil rather than a rolling motion. Due to the quasi-static nature of pad foot compaction, this configuration is comparable to the specific instances during field compaction when the pad is oriented vertically in the soil. This configuration is much easier to evaluate experimentally in a lab setting than a rolling motion, thus allowing for easy comparison of results between modeling, lab testing, and a portion of field testing. To model this loading, the pad model was rigidly fixed around the rim that is welded to the drum ($z = 0$ in Figure 3) and variable loads were applied on the outer faces in contact with the soil Figure 4.

Loading was applied to the pad that would mimic different soils (i.e. sand, silt, clay). There is a base of theoretical and experimental knowledge regarding soil behavior that guided loading parameters in this regard. Soil type influences the distribution of contact stress on a surface. Terzaghi[5] suggested that when interacting with a rigid surface (such as a compactor pad), soils with cohesion exhibit an "inverse parabolic" contact stress distribution (CSD), i.e. contact stresses reach a maximum at outer edges and a minimum at the center. Conversely, cohesionless soils exhibit a "parabolic" distribution, i.e. contact stresses reach a maximum at the center and dissipate toward the edges. This theory was confirmed experimentally by Schultze[6] and Mooney & Miller[7] with the findings indicating that the maximum and minimum stresses could be as much as twice and one-half of the average contact stress, respectively. Therefore, our model simulations included three loading configurations: parabolic, uniform, and inverse parabolic, with the non-uniform distributions having maximum and minimum loads of twice and one-half the average contact stress. These loading configurations are presented in Figure 4. The loading was applied normal the bottom face and bottom fillet of the pad, as shown in Figure 4d, which represents 9 mm of soil penetration. This degree of penetration is representative of a stiff soil, which would typically be encountered after several roller passes.

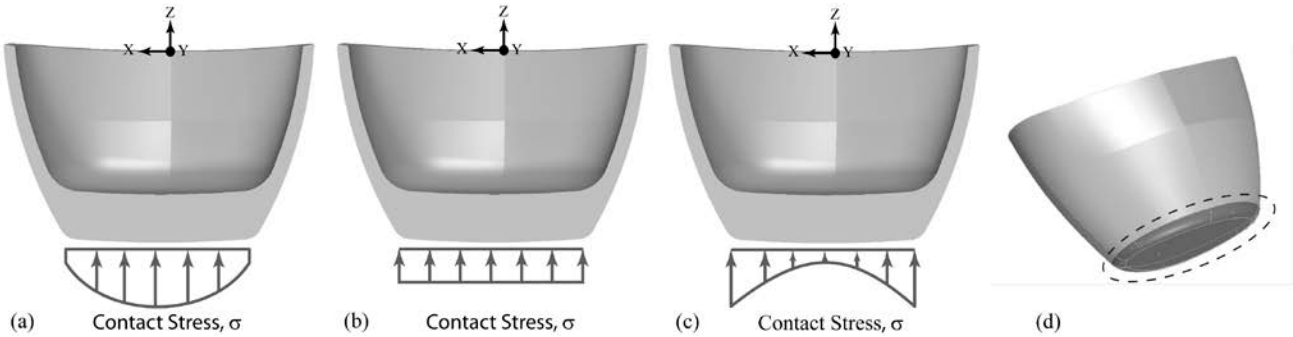

Figure 4. Loading on pad model. Contact stress distributions used in FEA include: (a) parabolic simulates cohesionless soils, (b) uniform simulates an intermediate soil, and (c) inverse parabolic simulates a cohesive soil. The loaded surfaces are highlighted in (d).

The magnitude of force applied to a pad was determined based on pad-drum geometry, and observations of field compaction. It was estimated that during initial passes in uncompacted soil, as many as 27 pads would share the weight of the machine, in addition to the drum itself contacting the ground and carrying weight. In compacted soil (after multiple passes), the weight of the machine would be shared by approximately 13 pads. These observations provide an estimated range of 0.5 kN- 9 kN of total normal force applied to an individual pad during normal compaction operations.

The standard or 'stock' pads provided by the manufacturer required modification to yield measurable strain levels under the full range of rolling conditions. Specifically, a pocket was machined out of the bottom face that removed an average of 19 mm of thickness out of the standard 33 mm of thickness, as shown in Figure 5. No modifications to the sidewalls were made.

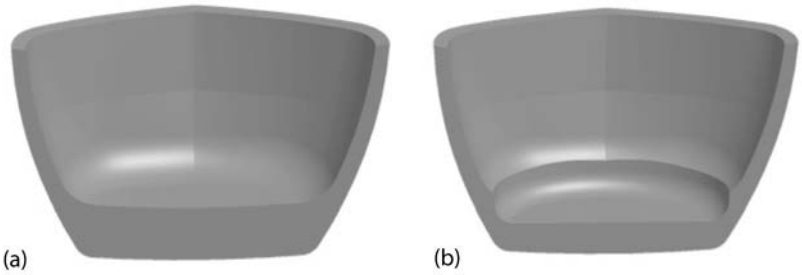

Figure 5. Cross section of an unmodified pad and a modified pad design. The modification provides increased strain magnitudes over the stock pad design.

The model parameters discussed in this section allowed us to simulate various soil conditions experienced during compaction. The following section presents the results from the FEA.

3 ANALYSIS OF PAD STRAIN MODELING

This section presents the FEA results concerning pad strain behavior under different loading scenarios. The results show that strains throughout the pad are sensitive to CSD and applied force.

For the prescribed loading conditions, normal and shear strains in the defined coordinate system were investigated. The normal strains are presented in Figure 6 and follow the solid mechanics convention, i.e. positive indicates tension, negative indicates compression. The shear strains did not produce any significant trends, and thus are not presented graphically. The maximum and minimum normal strains were elicited by the parabolic CSD, and were 81.7με (ε_{yy}) and -89.6με (ε_{zz}) respectively. Strains for a uniform CSD were approximately 70% lower, and for an inverse parabolic CSD were 90% lower. The pad experienced particularly high tensile strains in the center of the bottom face of the pad, and particularly high compressive strains in the fillet encircling the machined pocket and in the sidewalls.

Strains in the pad scale proportionally with the load magnitude because this is a purely elastic analysis. Therefore, if the CSD is known, then the strain from any point on the pad can provide the load magnitude. However, it unknown if CSD can be determined in the field during compaction. Ideally, total normal force could be measured without knowledge of the CSD. The principle of Saint Venant states that at a substantial distance from an applied load, the strain in the part is independent of the load distribution[13]. Unfortunately, the pad does not possess nearly sufficient length in the dimension parallel to the load (z-axis) to allow for Saint Venant's principle to be fully realized. Even at the rim of the pad, the ε_{zz} strain distribution is highly dependent on CSD. Still, ε_{zz} in the sidewalls is less sensitive to CSD than other strains in the pad. The vertical distribution of ε_{zz} along the sidewalls indicates a peak at approximately 73 mm from the rim, which would allow for maximum signal-noise ratio for sensors. A cross section of the ε_{zz} strain distribution at this point for the three CSD scenarios is provided in Figure 7b.

FE analysis shows that strains throughout the pad are sensitive to CSD. Strain magnitudes are clearly affected by CSD, but also by total applied load. Strain gradients, however, are only affected by CSD. The most pronounced connection between pad strain gradients and CSD can be seen in the inside bottom face of the pad (where pocket was machined out) in Figure 6, by comparing across any single row of pictures. The bottom face strain gradients were steepest for a parabolic CSD, less steep for a uniform CSD, and slightly inverted for an inverse parabolic CSD. The strains undergo the greatest change along the largest dimension of the bottom face, which in this case is the x-axis. The ε_{xx} strain gradient in the bottom face along the x-axis are shown in Figure 7a. This trend is consistent with elastic theory for a fixed-fixed plate (analogous to the bottom wall of the pad) under non-uniform pressure distribution[12].

The trends discovered in this analysis provide the foundation for choosing locations to place strain gages in order to measure total normal load and CSD.

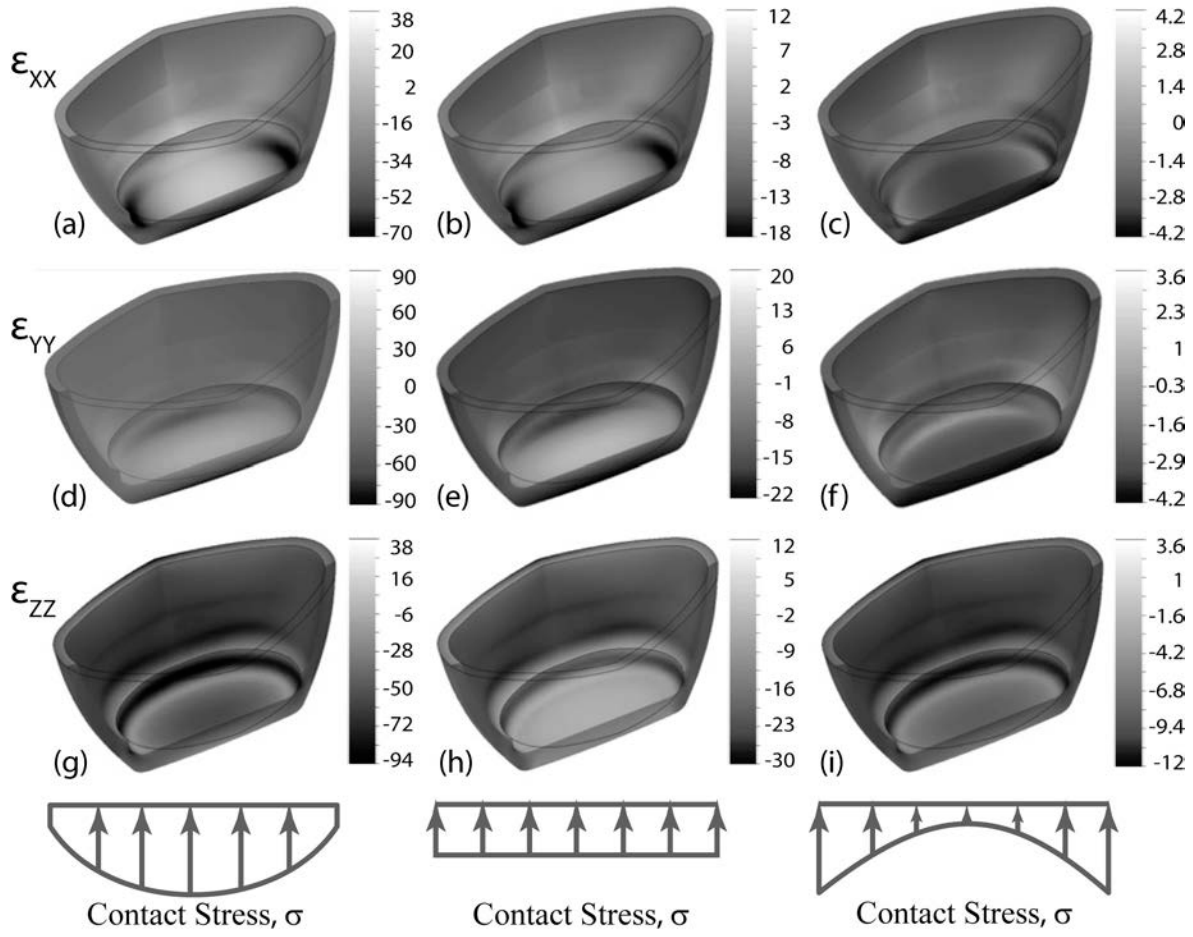

Figure 6. Normal strains (in microstrain) for a Caterpillar pad at maximum load magnitude, following solid mechanics convention: tension is positive and compression is negative. (a) ε_{xx} for parabolic CSD, (b) ε_{xx} for uniform CSD, (c) ε_{xx} for inverse parabolic CSD, (d) ε_{yy} for parabolic CSD, (e) ε_{yy} for uniform CSD, (f) ε_{yy} for inverse parabolic CSD, (g) ε_{zz} for parabolic CSD, (h) ε_{zz} for uniform CSD, and (i) ε_{zz} for inverse parablic CSD

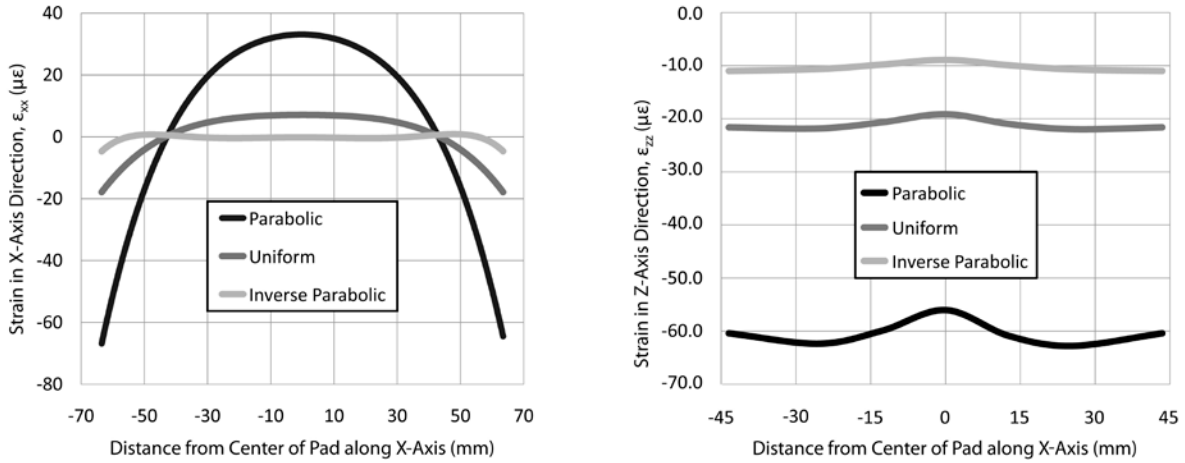

Figure 7. Strain trends along (a) bottom face and (b) 73 mm sidewall of the pad for different contact stress distributions at a total applied load of 9 kN.

4 DETERMINING PLACEMENTS OF STRAIN GAGES

Several considerations were taken into account when choosing and placing strain gages, including the physical footprint of the gage, measurement axes, and placement method. The reading from a gage represents the average strain over the gage area, i.e., it is not a point measurement. The pad strain field exhibited significant gradients, e.g., ε_{xx} 4.1 με/mm, and therefore, gage lengths were limited to 6.3 mm. The gages used include single uniaxial gages and rosettes (3 overlapping gages). In addition to considerations for the gage itself, there are considerations for the method of fixing the gages to the part. Pads are typically welded onto a drum, which introduces high temperatures to specific regions of the pad. Some of the gages were chosen to be located near a weld point and had to be fixed to the pad with high temperature epoxy and cured in place.

There are two specific trends we identified through FEA that we wish to capture with the gages. These include the sensitivity of sidewall ε_{zz} to total normal force, and the sensitivity of the bottom inside face ε_{xx} to CSD and total normal force. Both of these trends can be discretely measured with strain gages.

FEA showed ε_{zz} in the sidewall to be sensitive to the total normal force, and less sensitive to CSD than the rest of the pad. The instrumentation for this trend included placing gages on the sidewall 73mm down from the rim of the pad on 12.5 mm centers as shown in Figure 8a. The notation describes the axes of measurement and distance from the Z-Y plane, i.e. $\varepsilon_{zz}(15)$ is a normal strain measurement most closely aligned with the Z-axis 15 millimeters from the Z-Y plane. The gage placements include both sides of the pad, i.e. mirrored about the X-Z plane, which is a plane of symmetry for the loading conditions described. The signals from two symmetric gages are added together to double the signal to noise ratio. The sidewall gage locations are close enough to the weld joint of the pad to suspect temperatures that would surpass the rating on standard strain gage adhesive (>200°C). In place of the standard glue, a high temperature epoxy was used to fix the gages.

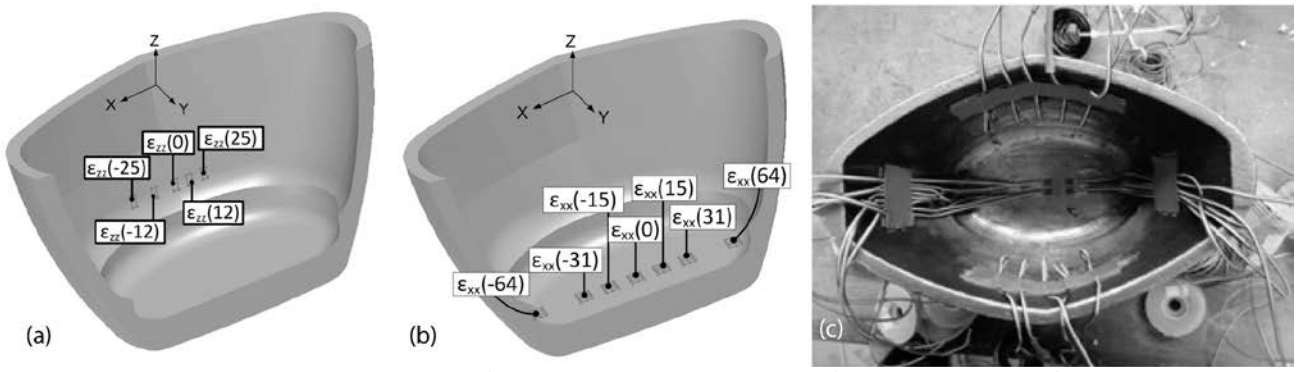

Figure 8. Strain gage arrays on the (a) sidewall of the pad help describe total normal force, and (b) bottom of the pad help describe total normal force and CSD. Gage notation specifies approximate axis of measurement and distance from Y-Z plane in mm. (c) Shows the gages installed on a modified pad.

The distribution of ε_{xx} on the bottom face of the pad is highly sensitive to the CSD and total normal force. To capture the characteristics of this trend a fairly dense gage array was employed. The array includes seven gages in total, shown in Figure 8b, with gages distributed on 15 mm centers except for the outer most gages. These outer gages measure the strain on the rounded surface of the fillet, which is not purely ε_{xx}, but is a point of interest as seen in Figure 6. The gage array falls along the X-Z plane, which is a plane of symmetry for the pad during the loading conditions discussed in this paper. Instead of a single gage being placed directly on the centerline, two complementary gages were placed mirrored about the X-Z plane. The signals of these gages can then be combined to double the signal to noise ratio.

The twelve gage locations discussed here provide definitive information about the CSD and the total normal force on the pad. Measuring both CSD and total normal load is critical to determining soil stiffness and modulus. While these results concern a Caterpillar pad, the results are fairly transportable to other manufacturer's pads, due to the similar geometry characteristics of a trapezoidal profile and hollow interior.

5 CONCLUSIONS

Towards the development of a real-time soil compaction monitoring system for static pad foot compaction, we have taken the first steps to create a pad sensor to measure soil stiffness. The system is based on the fact that pad loading changes throughout compaction, and that this loading can be sensed through measuring pad strain. Pad foot soil compactor pads were analyzed with FEA to investigate strain fields with relation to loading. Loading variables included total load magnitude and load distribution. Two strain trends were identified through FEA that provide information about the loading of the pad: ε_{zz} in the sidewall is sensitive to total normal load, and ε_{xx} on the bottom inside face of the pad are sensitive to total normal load and CSD.

Strain gage locations were determined based the identified trends, resulting in twelve gage placements. This included five gages on the sidewall to measure ε_{zz}, and seven gages on the bottom inside face of the pad to measure ε_{zz}. This instrumentation pattern provides definitive information on CSD and total normal force, both of which are necessary for the real-time soil stiffness measurement system proposed. A pad has been instrumented in the described fashion, and future work will include experimental studies in the lab and field to further investigate pad strain behavior.

ACKNOWLEDGMENTS

Funding for this research is provided by the FHWA Exploratory Advanced Research Program (No. DTFH61-07-H-00036). Additional support is provided by the National Science Foundation (IGERT). The participation of industry partners Caterpillar and Case Construction, as well as the Colorado Department of Transportation and the Denver Transit Construction Group is gratefully appreciated.

REFERENCES

[1] Mooney, M., Rinehart, R., White, D., Vennapusa, P., Facas, N. and Musimbi, O., “Intelligent Soil Compaction Systems,” NCHRP Project 21-09 Final Report, Transportation Research Board (2010)

[2] Chang, G., et. al., “IC Field Demonstration on Cohesive Subgrade, Stabilized Subgrade, and Flex Base,” FHWA/ TPF Research Project Report (2008)

[3] LandPac, Website http://www.landpac.co.za/, accessed 31 Jan 2010

[4] White, D. et. al., “Field Evaluation of Compaction Monitoring Technology: Phase II,” Final Report to Iowa Department of Transportation (2006)

[5] Terzaghi, K. and Ralph B. P., [Soil Mechanics in Engineering Practice], John Wiley and Sons, New York (1948)

[6] Schultze, E., “Distribution of Stress Beneath a Rigid Foundation,” Proc. 5th Int. Conf. on Soil Mechanics and Foundation Engrg. 1, 807 (1961)

[7] Mooney, M. A. and Miller, P. K., “Analysis of Light Weight Deflectometer Test Based on In-Situ Stress and Strain Response,” J. Geotechnical and Geoenvironmental Engrg. ASCE 135(2), 199-208 (2009)

[8] Budynas, R., [Advanced Strength and Applied Stress Analysis], McGraw-Hill, 2nd edition, Boston (1998)

[9] Toupin, R. A., “Saint-Venant's Principle,” Archive for Rational Mechanics and Analysis 18, 83-96 (1965)